James M. Dominguez II,[1] Mark A. Yorek,[2,3] and Maria B. Grant[4]

Combination Therapies Prevent the Neuropathic, Proinflammatory Characteristics of Bone Marrow in Streptozotocin-Induced Diabetic Rats

Diabetes 2015;64:643–653 | DOI: 10.2337/db14-0433

We previously showed that peripheral neuropathy of the bone marrow was associated with loss of circadian rhythmicity of stem/progenitor cell release into the circulation. Bone marrow neuropathy results in dramatic changes in hematopoiesis that lead to microvascular complications, inflammation, and reduced endothelial repair. This series of events represents early pathogenesis before development of diabetic retinopathy. In this study we characterized early alterations within the bone marrow of streptozotocin (STZ)-induced diabetic rats following treatments that prevent experimental peripheral neuropathy. We asked whether bone marrow neuropathy and the associated bone marrow pathology were reversed with treatments that prevent peripheral neuropathy. Three strategies were tested: inhibition of neutral endopeptidase, inhibition of aldose reductase plus lipoic acid supplementation, and insulin therapy with antioxidants. All strategies prevented loss of nerve conduction velocity resulting from STZ-induced diabetes and corrected the STZ-induced diabetes–associated increase of immunoreactivity of neuropeptide Y, tyrosine hydroxylase, and somatostatin. The treatments also reduced concentrations of interleukin-1β, granulocyte colony-stimulating factor, and matrix metalloproteinase 2 in STZ-induced diabetic bone marrow supernatant and decreased the expression of NADPH oxidase 2, nitric oxide synthase 2, and nuclear factor-κB1 mRNA in bone marrow progenitor cells. These therapies represent novel approaches to attenuate the diabetic phenotype within the bone marrow and may constitute an important therapeutic strategy for diabetic microvascular complications.

An estimated 29.1 million people in the U.S. have diabetes mellitus, which equates to 9.3% of the population (1). Of patients with diabetes, 60% to 70% have neuropathy, which manifests as a wide range of symptoms depending on the affected nerves and the targets of innervation. More than half of all major lower-limb amputations in the U.S. are associated with diabetes (2).

Diabetic neuropathy is multifactorial but has a pathogenesis strongly associated with microvascular dysfunction, increased polyol pathway activation, elevated reactive oxygen species (ROS), and chronic inflammation (3,4). Pharmacological strategies exist to target this pathology. Inhibition of neutral endopeptidase permits the accumulation of vasodilatory peptides and decreases oxidative stress, which preserves vascular function and prevents diabetic neuropathy (4). Inhibition of aldose reductase improves neuropathy by attenuating the diabetes-associated decline of nerve conduction velocity (3,5) and hyperglycemia-induced oxidative stress, in part by maintaining glutathione concentrations (6). Lipoic acid (LA) decreases oxidative stress by direct free radical scavenging and by regenerating other intracellular antioxidants, including glutathione (7); it also has been shown to improve diabetic neuropathy by not only

[1]Department of Pharmacology and Therapeutics, University of Florida, Gainesville, FL
[2]Department of Veterans Affairs, Iowa City VA Health Care System, Iowa City, IA
[3]Department of Internal Medicine, University of Iowa, Iowa City, IA
[4]Department of Ophthalmology, Indiana University School of Medicine, Indianapolis, IN
Corresponding author: Maria B. Grant, mabgrant@iupui.edu.

Received 18 March 2014 and accepted 2 September 2014.

This article contains Supplementary Data online at http://diabetes.diabetesjournals.org/lookup/suppl/doi:10.2337/db14-0433/-/DC1.

attenuating oxidative stress (8) but also normalizing endoneurial blood flow (9) and improving vascular function (10). Similarly, omega-3 polyunsaturated fatty acids (ω-3 PUFAs), although controversial, have anti-inflammatory effects and attenuate diabetic symptoms (c.f. ref. 11).

Innervation of the bone marrow regulates the release of progenitor and immune cell populations from the bone marrow. Activation of sympathetic noradrenergic nerves permits vascular progenitor cells and immune cells to enter the circulation and perform systemic surveillance of peripheral tissues (12). We previously demonstrated that diabetic neuropathy manifests in the bone marrow, resulting in decreased total innervation, sensory innervation, and adrenergic innervation, which alter stromal cell secretion of cytokines and growth factors, leading to a shift toward increased generation of myeloid cells but reduced numbers of endothelial progenitor cells (13–15). Both streptozotocin (STZ)-induced diabetic and type 2 diabetic (T2D) rats exhibited bone marrow neuropathy, which was concluded to contribute to diabetic retinopathy (14).

The purpose of this study was to evaluate the changes found in the bone marrow microenvironment of STZ-induced diabetic rats following administration of selected treatments that have been shown to prevent diabetic peripheral neuropathy. We assessed the presence of neuropathic changes by testing thermal nociceptive response, motor nerve conduction velocity (MNCV), and sensory nerve conduction velocity (SNCV) in the sciatic nerve. We evaluated the bone marrow microenvironment in STZ-induced diabetic rats by examining changes in neural immunoreactivity, growth factors, and cytokines within the bone marrow and by measuring changes in gene expression in bone marrow–derived progenitor cells.

RESEARCH DESIGN AND METHODS

Pharmacological Agents

Unless stated otherwise, all chemicals used in these studies were obtained from Sigma Chemical (St. Louis, MO). Ilepatril (Ile) was a generous gift from Dr. Jurgen Punter (Sanofi, Paris, France). Fidarestat (Fid) was a generous gift from Sanwa Kagaku Kenkyusho (Kariya, Aichi, Japan). Insulin was purchased from Sanofi.

Animal Studies

Male, 12-week-old Sprague-Dawley rats (Harlan, Indianapolis, IN) were housed in a certified animal care facility, with food (#7001; Harlan Teklad, Madison, WI) and water provided ad libitum. All institutional (approval ACURF no. 1202032) and National Institutes of Health guidelines for use of animals were followed. Diabetes was induced by intraperitoneal injection of STZ (55 mg/kg in 0.9% sodium chloride, adjusted to pH 4.0, with 0.2 mol/L sodium citrate). Control rats were injected with vehicle alone. Diabetes was verified 48 h later by evaluating blood glucose concentrations using glucose dehydrogenase–based reagent strips (Aviva Accu-Chek; Roche, Mannheim, Germany). Rats with a blood glucose concentration of ≥300 mg/dL (11.1 mmol/L) were considered diabetic.

Treatment Conditions

Two weeks after the verification of diabetes, five groups were established: *1*) untreated nondiabetic (Con group, n = 8); *2*) untreated diabetic (DM group, n = 11); *3*) diabetic treated with Ile (DM + Ile group, n = 10); *4*) diabetic treated with Fid and LA (DM + Fid + LA group, n = 10); and *5*) diabetic treated with insulin and menhaden oil (Menh) (DM + Ins + Menh group, n = 7). The treatment dosages are listed in Supplementary Table 1. With the exception of insulin and Menh, all treatment compounds were mixed in the meal form of the diet, which was subsequently pelleted and dried in a vacuum oven for 16 h at 37°C. The diet containing Menh was purchased from Research Diets (New Brunswick, NJ). The treatment phase of the study lasted 6 weeks, and the total duration of diabetes was 8 weeks. Elevated glycated hemoglobin was significantly attenuated only in the DM + Ins + Menh group.

Thermal Nociceptive Response

The day before the terminal studies, thermal nociceptive response in the hind paw was measured using the Hargreaves method, as previously described (16). Four measurements were made for each hind paw, and the mean of the measurements was used as the response time. Afterward, MNCV and SNCV in the sciatic nerve were determined.

MNCV and SNCV

MNCV was determined as previously described using a noninvasive procedure in the sciatic-posterior tibial conducting system in a temperature-controlled environment (16). SNCV was determined using the digital nerve to the second toe, as previously described (16).

Isolation of Thy-1$^+$ Cells From Bone Marrow

Rats were anesthetized with 50 mg/kg intraperitoneal Nembutal (Abbott Laboratories, North Chicago, IL) and killed by exsanguination. After death, hind limb bones were removed, placed in 10-mL containers filled with PBS, packed on wet ice, and shipped overnight to the University of Florida. Upon receipt, the femoral marrow compartment was flushed with 10 mL of PBS and the cells pelleted by centrifugation. The supernatant was flash-frozen for later cytokine quantification. The cells then were treated with ammonium chloride (STEMCELL Technologies Inc., Vancouver, BC, Canada) to remove any contaminating red blood cells and resuspended in PBS per the instructions of a customized negative-selection kit (STEMCELL Technologies) used to magnetically deplete CD4$^+$, CD5$^+$, CD8a$^+$, and OX-43$^+$ cells. The cells then were enriched for CD90$^+$ (Thy-1) cells using a positive selection magnet separation kit (STEMCELL Technologies) with an antibody for CD90/Thy-1.

Cytokine Quantification

Concentrations of cytokines in the bone marrow supernatant were determined using microsphere-based suspension

microarray technology (AssayGate, Ijamsville, MD). This methodology is the Luminex bead-based immunoassay platform. In brief, multiple analytes from a single sample of bone marrow supernatant were determined using the Bio-Plex 200 Bead Reader System (Bio-Rad, Hercules, CA). Microparticles were conjugated to differing concentrations of two fluorophores to generate distinct bead sets. Each bead set was coated with capture antibody specific for one analyte. Captured analyte was detected using a biotinylated detection antibody and streptavidin–phycoerythrin. The bead analyzer was a dual-laser, flow-based sorting and detection platform. One laser was bead-specific and the other determined the magnitude of phycoerythrin-derived signal, which is in direct proportion to the amount of analyte bound. Each sample was tested in duplicate. The results were expressed as picograms per milliliter. Analyte concentrations below the threshold of detection were excluded from the analysis.

Real-Time Quantitative RT-PCR

Bone marrow–derived Thy-1$^+$ cells were homogenized in TRIzol reagent (Invitrogen), and RNA was isolated according to the manufacturer's instructions. First-strand cDNA was synthesized from isolated RNA using an iScript cDNA synthesis kit (Bio-Rad). Prepared cDNA was mixed with Gene Expression Master Mix (Applied Biosystems, Carlsbad, CA) and the respective gene-specific TaqMan assays (Life Technologies) and subjected to real-time PCR quantification using the 7500 Fast Real-Time PCR System (Applied Biosystems). Genes of interest included NADPH oxidase-2 (NOX-2, Rn00576710_m1), intracellular adhesion molecule-1 (ICAM, Rn00564227_m1), interleukin (IL)-6 (IL-6, Rn01410330_m1), IL-1β (Rn00580432_m1), nuclear factor κ light chain enhancer of activated B cells (NF-κB1, Rn01399583_m1), inducible nitric oxide synthase (NOS-2, Rn00561646_m1), Toll-like receptor 4 (TLR-4, Rn00569848_m1), angiotensin II receptor type 1a (AgtR1a, Rn02758772_s1), and angiotensin I–converting enzyme 2 (ACE2, Rn01416293_m1). All reactions were performed in triplicate. Relative mRNA levels were calculated using the comparative threshold method, normalized to mitochondrial ribosomal protein L-19 (MRPL-19, Rn01533663_m1).

Immunohistochemistry

Formalin-fixed femurs were processed as previously described (14). Briefly, bones were decalcified, embedded in paraffin, and sectioned on a rotary microtome at 4 μm. Sections were placed on adhesive slides, deparaffinized, and submitted to antigen-retrieval protocols (Supplementary Table 2). Following pretreatments, standard avidin-biotin complex staining steps were performed at room temperature using a Dako Autostainer. After blocking nonspecific protein with nonimmune goat serum (Vector Laboratories, Burlingame, CA), sections were incubated with an avidin (Vector Laboratories)/biotin (Sigma-Aldrich) blocking system. Sections were incubated with antibodies (Supplementary Table 3) followed by R.T.U. VectaStain Elite ABC Reagent (Vector) and were developed with NovaRED (Vector Laboratories) followed by counterstain in Gill 2 hematoxylin (Richard Allen, Kalamazoo, MI). Slides then were dehydrated, cleared, and placed on a slide under a coverslip with Flotex Permount mounting media.

Aperio and Positive Pixel Count Algorithm

Stained femurs on slides were scanned using an Aperio CS slide scanning system with a Spectrum Plus information management system (Aperio Technologies, Inc., Vista, CA). The ImageScope program (Aperio) was used to quantify positive staining in two regions of marrow (distal middle and middle) using the Positive Pixel Count algorithm (Aperio). Positive pixels were determined by a range of hues, saturations, and intensities of NovaRED. Negative controls for all targets were analyzed to ensure that the algorithm detected minimal positive pixels. Adiposity of the bone marrow was assessed in a representative region within the middle distal femur that spanned from the medial cortex to the lateral cortex and constituted an area between 1 and 1.5 mm^2. Adipose remains unstained and is thus not considered positive or negative by the algorithm. Therefore, we subtracted the area of positive and negative pixilation from the total area of the selected region. We were careful to select regions devoid of nonstained artifact, for example, tears in the tissue resulting from processing.

Data Analysis

All data were analyzed for outliers before treatment comparisons. Comparisons between the groups were assessed using a one-way ANOVA followed by the Tukey post hoc test. $P < 0.05$ was considered significant.

RESULTS

Morphologic Characteristics of Experimental Rats

Blood glucose, glycated hemoglobin, and body weight before and after the study are shown in Table 1. STZ-induced diabetes was associated with decreased body weight in all groups, which was prevented only in the DM + Ins + Menh group. Likewise, blood glucose and glycated hemoglobin were elevated in all STZ-induced diabetic groups except DM + Ins + Menh.

Thermal Nociceptive Response and Nerve Conduction Velocities

Neuropathy results in altered conduction velocities and dampened sensitivity to noxious stimuli. Compared with nondiabetic controls, untreated diabetes was associated with decreased MNCV and SNCV in the sciatic nerve conducting system and delayed response to noxious heat. All treatment conditions prevented nerve dysfunction associated with STZ-induced diabetes (Table 2).

Quantification of Tyrosine Hydroxylase Immunoreactivity

Tyrosine hydroxylase (TH) is a rate-limiting enzyme in catecholamine biosynthesis (17), and its activity is a measure of the number of sympathetic neurons and an index of sympathetic nervous system activity (18). Figure 1*A* shows representative TH staining in the distal middle

Table 1—Effect of treating diabetic rats with Ile, Fid + LA, or Ins + Menh on change in body weight, blood glucose, and HbA_{1c}

	Con (n = 9)	DM (n = 10)	DM + Ile (n = 10)	DM + Fid + LA (n = 10)	DM + Ins + Menh (n = 10)
Weight (g)					
Start	337 ± 4	337 ± 3	338 ± 3	338 ± 2	337 ± 2
End	445 ± 6	357 ± 14*	360 ± 16*	315 ± 13*	428 ± 5†
Blood glucose (mg/dL)	141 ± 5	584 ± 13*	539 ± 27*	515 ± 19*	205 ± 52†
HbA_{1c} (%)	7.3 ± 0.5	14.3 ± 1.8*	12.4 ± 1.0*	13.2 ± 1.5*	8.8 ± 1.5†
HbA_{1c} (mmol/mol)	56 ± 3.8	133 ± 16.7*	112 ± 9.0*	121 ± 13.8*	73 ± 12.4†

Data are presented as mean ± SEM. *$P < 0.05$ compared with control rats; †$P < 0.05$ compared with diabetic rats. Values in parentheses indicate the number of experimental animals.

femoral marrow before (top gray images) and after analysis (bottom blue images) by Aperio using the Positive Pixel Count algorithm. Positive staining is depicted by yellow (weak positive), orange (middle positive), and red (strong positive). Semiquantification of the staining for TH revealed that STZ-induced diabetes was associated with an increased ratio of strong-positive immunoreactivity (i.e., Nsr = [number of strong-positive pixels] ÷ [number of all positive pixels]), which is shown in Fig. 1*B*. We interpret this finding as an indicator of increased neuronal injury and subsequent successful repair or preemptive neurogenesis. The increased strong-positive immunoreactivity was significantly attenuated in the DM + Ile and the DM + Fid + LA groups.

Quantification of Somatostatin Immunoreactivity

Somatostatin (SST) is a neurotransmitter that exerts anti-inflammatory and immunosuppressive effects (19). Immunostaining for SST (Fig. 2*A*) revealed a trend similar to that of TH. STZ-induced diabetes was associated with increased ratio of strong-positive immunoreactivity in the femoral marrow, which was attenuated only in the DM + Fid + LA group (Fig. 2*B*).

Quantification of Neuropeptide Y Immunoreactivity

Neuropeptide tyrosine (NPY) functions to increase progenitor cell populations and maintain their undifferentiated status in the bone marrow (20). NPY immunostaining in STZ-induced diabetes also was associated with an increased ratio of strong-positive immunoreactivity in the femoral marrow (Fig. 3*A*), analogous to TH and SST. The increase of NPY immunoreactivity associated with STZ-induced diabetes was attenuated in the DM + Fid + LA and the DM + Ins + Menh groups (Fig. 3*B*).

Quantification of Calcitonin Gene-Related Peptide and 8-Hydroxy-2′-Deoxyguanosine Immunoreactivity

In an effort to assess whether Ile decreased vasodilatory peptide degradation, we performed immunohistochemistry for the peptide and neurotransmitter calcitonin gene-related peptide (CGRP). However, we did not detect any significant differences within the bone marrow between the experimental groups (Supplementary Fig. 1).

A possible mechanism for the beneficial effect of Fid + LA and Menh + Ins treatments is reduction of oxidative stress. We measured concentrations of 8-hydroxy-2′-deoxyguanosine, a product of DNA oxidation, within the bone marrow; however, we did not detect any differences in the immunoreactivity between experimental groups.

Bone Marrow Adiposity

Marrow adipose is proposed to have multiple functions, including autocrine/paracrine/endocrine support as well as a regulatory role in stem cell differentiation. STZ-induced diabetes was associated with a loss of bone marrow adiposity, which corroborated our previous findings (13). The loss of femoral marrow adiposity associated with STZ-induced diabetes was prevented in the DM + Ile and DM + Ins + Menh groups (Fig. 4).

Bone Marrow Cytokines

The supernatant from STZ-induced diabetic bone marrow was associated with elevated proinflammatory cytokines and proteases. Significant differences between groups were found for the following cytokines (picograms per milliliter): matrix metalloproteinase (MMP)-2 (Fig. 5*A*), IL-1β (Fig. 5*C*), macrophage colony-stimulating factor (Con group 4.24 ± 0.4 vs. DM group 5.24 ± 0.96), IGF-I (Con group 809.7 ± 329.9 vs. DM group 416.6 ± 195.9),

Table 2—Effect of treating diabetic rats with Ile, Fid + LA, or Ins + Menh on MNCV, SNCV, and thermal sensitivity

	Con (n = 9)	DM (n = 10)	DM + Ile (n = 10)	DM + Fid + LA (n = 10)	DM + Ins + Menh (n = 10)
MNCV (m/s)	56.2 ± 2.1	40.8 ± 1.2*	52.9 ± 1.6†	54.2 ± 1.4†	55.1 ± 3.0†
SNCV (m/s)	19.8 ± 0.3	17.6 ± 0.2*	19.0 ± 0.2†	18.9 ± 0.2†	19.6 ± 0.2†
Thermal sensitivity (s)	12.8 ± 0.6	19.0 ± 1.0*	12.3 ± 0.5†	13.2 ± 0.6†	11.1 ± 0.5†

Data are presented as mean ± SEM. *$P < 0.05$ compared with control rats; †$P < 0.05$ compared with diabetic rats. Values in parentheses indicate the number of experimental animals.

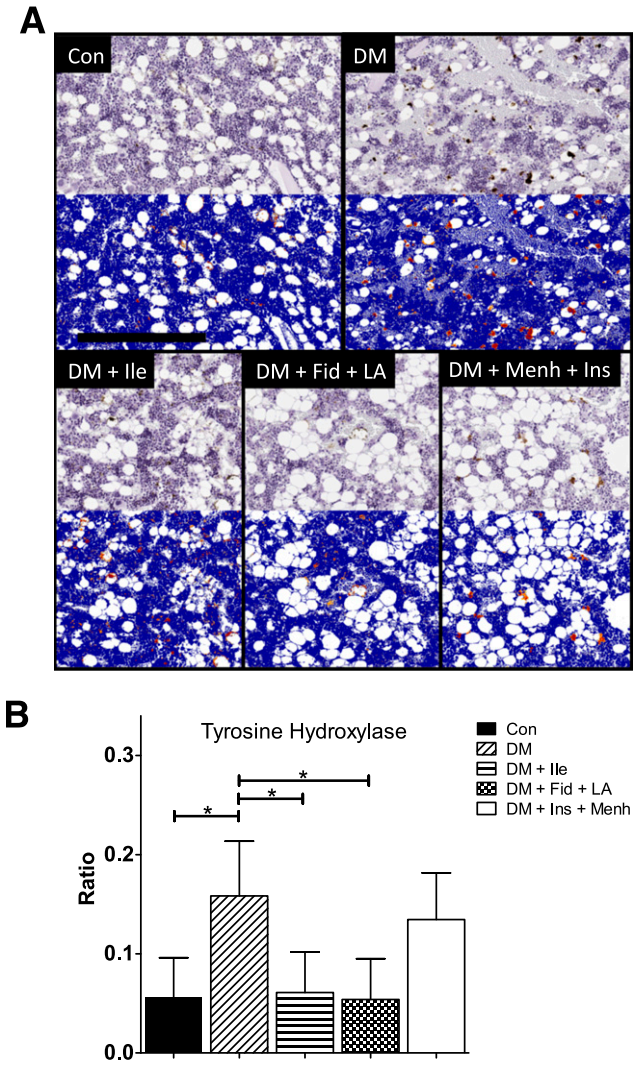

Figure 1—*A*: TH staining of middle distal femoral marrow. The images show representative TH staining before (top gray images) and after quantification (bottom blue images) by Aperio using the Positive Pixel Count algorithm. In the markup images, a positive stain is indicated by yellow (weak positive), orange (middle positive), and red (strong positive). There were 7–12 animals per group. Scale bar = 300 μM. *B*: Ratio of strong-positive TH pixels to total positive pixels in the middle distal femur. Data represent mean ± SD. *Significant differences between groups ($P < 0.05$).

IGF-binding protein-3 (DM group 39,760.8 ± 4,758.6 vs. DM + Fid + LA group 29,006.7 ± 4,574.1), IL-3 (DM group 47.5 ± 26.8 vs. DM + Ins + Menh group 230.9 ± 160.6), and IL-10 (DM group 89.41 ± 66.1 vs. Con group 16.56 ± 6.52, DM + Ile group 10.04 ± 0.01, DM + Fid + LA group 28.75 ± 14.5, and DM + Ins + Menh group 16.83 ± 12.69) ($P < 0.05$). No significant differences between groups were found for MMP-9, stem cell factor, stromal cell-derived factor 1a, granulocyte colony-stimulating factor, IL-6, tumor necrosis factor-α, or vascular endothelial growth factor. Despite the dramatic difference between groups for granulocyte/macrophage colony stimulating factor (GM-CSF) (Fig. 5*A*), we were not able to perform statistics because of the undetectably low concentrations from nearly all samples in the control and treated groups.

Progenitor Cell Gene Expression

STZ-induced diabetes was associated with a robust increase in proinflammatory gene expression in progenitor cells, which corroborated our previous findings (13). All treatment conditions prevented this STZ-induced diabetes–associated increase. Significant differences were found between groups for NOX-2 (Fig. 6*A*), NF-κB1 (Fig. 6*B*), and NOS-2 (Fig. 6*C*). No significant differences were found between groups for ACE2 (Supplementary Fig. 2), AgtR1a (Supplementary Fig. 3), IL-6, or TLR-4.

DISCUSSION

To our knowledge, this study is the first to demonstrate a reversal of diabetes-associated alterations within the bone marrow, despite hyperglycemia and hypoinsulinemia. The diabetic phenotype of the bone marrow was characterized by an increased proportion of strong-positive immunoreactivity for TH, SST, and NPY (Figs. 1–3). These changes are consistent with preemptive neurogenesis and/or compensatory repair (21,22) following injury. The diabetic phenotype of the bone marrow was further characterized by decreased marrow adiposity (Fig. 4), a highly proinflammatory bone marrow microenvironment (i.e., elevated IL-1β, MMP-2, and GM-CSF) (Fig. 5), and increased proinflammatory gene expression (i.e., NOX-2, NF-κB1, NOS-2) (Fig. 6) in bone marrow–derived progenitor cells. All therapies that we investigated prevented peripheral neuropathy (Table 2) and showed high efficacy in attenuating the respective STZ-induced diabetes–associated alterations of the bone marrow.

Currently approved and available therapies for diabetic neuropathy are symptomatic as opposed to disease modifying. With the exception of rigorous glycemic control, there is currently no approved treatment to reverse, or even slow, the progression of diabetic neuropathy. Vascular dysfunction and decreased endoneurial blood flow precede neuropathy (i.e., decreased nerve conduction velocity) in STZ-induced diabetic rats (4). Herein we identified novel ways to prevent regional neuropathic changes in the bone marrow in this type 1 diabetic (T1D) model.

One of the primary drug targets in this study was neutral endopeptidase, which metabolizes vasodilatory peptides including the natriuretic peptides, bradykinin, and CGRP. Inhibition of neutral endopeptidase with Ile attenuates STZ-induced diabetes–associated decline of endoneurial blood flow and subsequent neuropathy by preventing degradation of vasoactive peptides and decreasing oxidative stress (4). Consistent with previous studies of other tissues, we demonstrated that neutral endopeptidase inhibition prevents the development of bone marrow pathology associated with STZ-induced diabetes. However, we expected this treatment to facilitate the accumulation of CGRP concentrations in the bone marrow, which we did not observe. We also did not see an

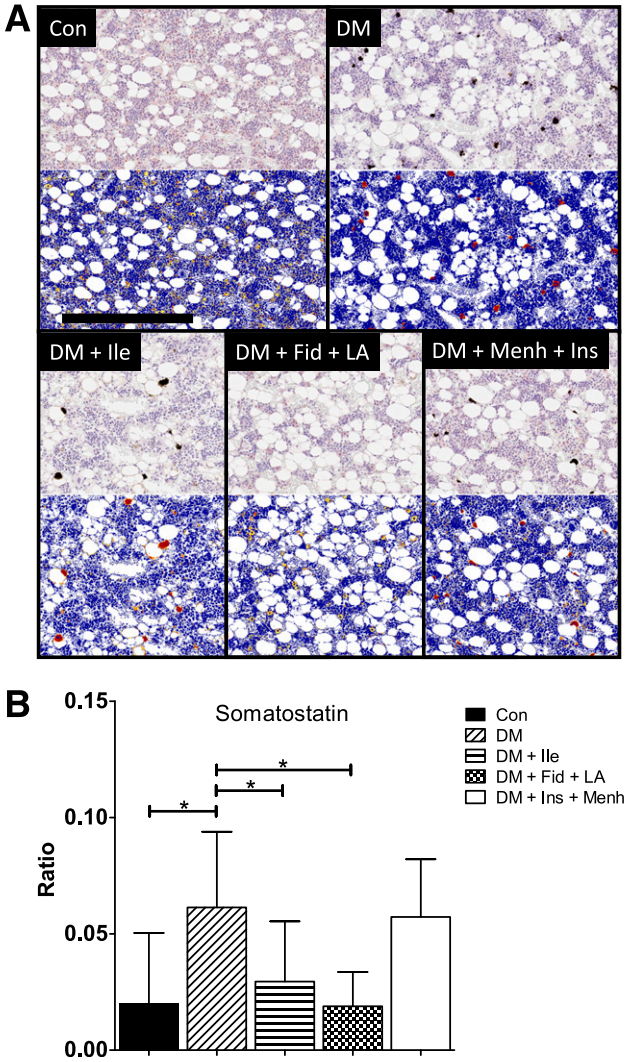

Figure 2—*A*: SST staining of middle distal femoral marrow. Images show representative SST staining before (top gray images) and after quantification (bottom blue images) by Aperio using the Positive Pixel Count algorithm. In the markup images, a positive stain is indicated by yellow (weak positive), orange (middle positive), and red (strong positive). There were 7–12 animals per group. Scale bar = 300 μM. *B*: Ratio of strong-positive SST pixels to total positive pixels in the middle distal femur. Data represent mean ± SD. *Significant differences between groups ($P < 0.05$).

increase of CGRP immunoreactivity in the untreated STZ-induced diabetic group, suggesting that CGRP-expressing neurons are not yet affected by the short duration of disease examined in this study. Although we did not detect differences for CGRP, neutral endopeptidase has many other targets that may have been improved with Ile, including bradykinin and the natriuretic peptides.

Ile is also an ACE inhibitor, which has vasomotor benefits. We found that ACE2, a component of the beneficial arm of the renin-angiotensin system, was highest in the Ile-treated group, followed by the Con group (Supplementary Fig. 2), as expected. In fact, ACE2 gene expression was detectable only in these two groups, rendering statistical comparison with untreated diabetes impossible. AgtR1a mRNA expression was highest in the DM followed by the Con groups and was undetectable in the DM + Ile group (Supplementary Fig. 3), as expected. However, none of these differences reached statistical significance.

Aldose reductase was another primary drug target chosen to attenuate oxidative stress. It is the first enzyme in the polyol pathway and catalyzes the reduction of glucose to sorbitol. Increased flux through the polyol pathway results in redox imbalance and oxidative stress due in part to lower concentrations of glutathione (6). Consequently, aldose reductase inhibition attenuates the T1D- and T2D-associated decline of nerve conduction velocity (3,5) and hyperglycemia-induced oxidative stress, maintaining glutathione concentrations (6). By maintaining redox balance, aldose reductase inhibition also decreases the expression of nuclear factor-κB (23), which is a redox-sensitive transcription factor that increases the production of proinflammatory cytokines and chemokines (24). These studies are consistent with our finding that aldose reductase inhibition prevented the STZ-induced diabetes–associated phenotype in the bone marrow.

Another drug target was LA, which in many clinical trials has shown efficacy for the treatment of chronic inflammatory diseases, including diabetes (10). More specifically, LA improves diabetic neuropathies via attenuating oxidative stress (8), normalizing endoneurial blood flow (9), and improving vascular function (25). The effect of LA on oxidative stress occurs by direct free radical scavenging and by the regeneration of other intracellular antioxidants, including glutathione (7). Here we showed that these effects extend to the STZ-induced diabetic bone marrow.

ω-3 PUFAs exhibit anti-inflammatory properties (c.f. ref. 11) and attenuate MMP-2 and MMP-9 expression in macrophages (26). Two notable ω-3 PUFAs are eicosapentaenoic acid and docosahexaenoic acid. Both readily incorporate into cell membranes, attenuate inflammation, and are enriched in Menh. We are aware of only one study that investigated the effect of Menh on peripheral neuropathy (16). Consistent with that study, our results suggest that Menh improved diabetic neuropathy, presumably because of the high proportion of ω-3 PUFAs and their anti-inflammatory effects.

In fact, all of our treatment conditions may have contributed to decreasing bone marrow inflammation. All three treatments corrected the increase of bone marrow GM-CSF associated with STZ-induced diabetes. Experimentally, monocytes/macrophages generated ex vivo in the presence of GM-CSF are skewed toward the proinflammatory M1 phenotype (27–29). In addition, GM-CSF and IL-1β positively regulate one another to promote inflammation (30,31). Therefore, suppressing GM-CSF would be expected to attenuate the production of proinflammatory monocytes/macrophages.

We also observed increased progenitor cell expression of mRNA for NOS-2 and NOX-2 in STZ-induced diabetes,

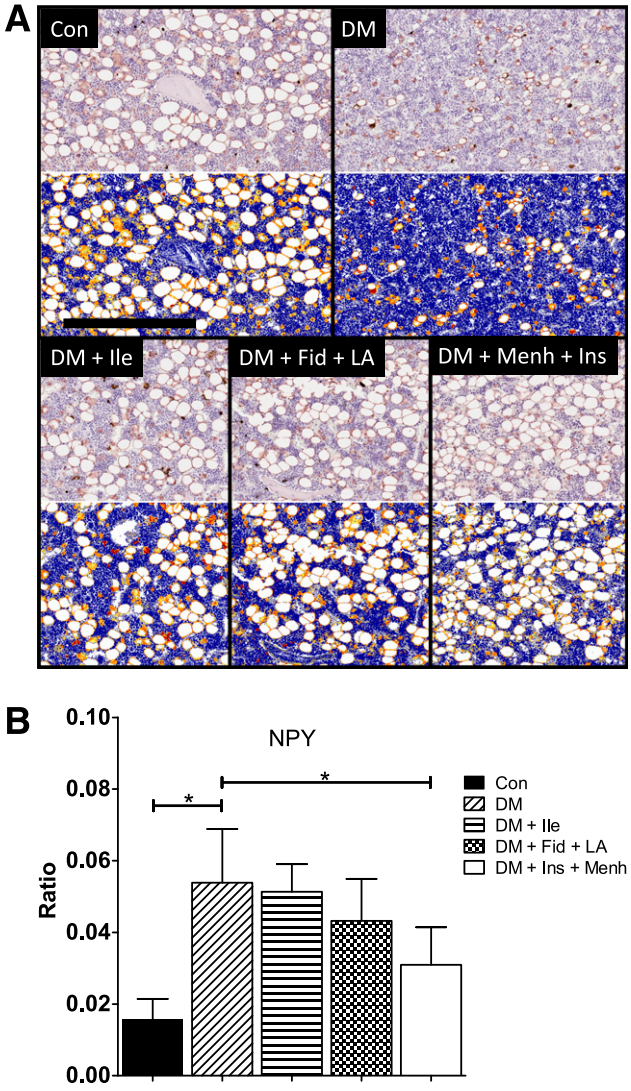

Figure 3—*A*: NPY staining of middle distal femoral marrow. Images show representative NPY staining before (top gray images) and after quantification (bottom blue images) by Aperio using the Positive Pixel Count algorithm. In the markup images, a positive stain is indicated by yellow (weak positive), orange (middle positive), and red (strong positive). There were 7–12 animals per group. Scale bar = 300 μM. *B*: Ratio of strong-positive NPY pixels to total positive pixels in the middle distal femur. Data represent mean ± SD. *Significant differences between groups ($P < 0.05$).

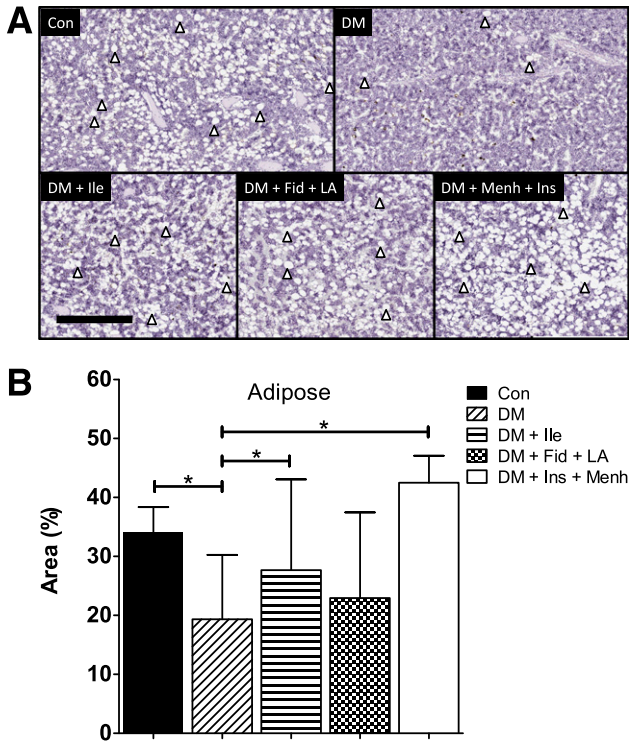

Figure 4—*A*: Treatments restore bone marrow adiposity. Adipocytes remain unstained in sections of middle distal femur stained with hematoxylin and eosin; they appear as white ovals and are indicated by arrowheads. Scale bar = 500 μM. *B*: Quantification of femoral marrow adiposity. Area of adiposity was determined by subtracting the area of positive and negative pixilation from the total area of a designated region. Data represent mean ± SD. *Significant differences between groups ($P < 0.05$).

which was corrected toward nondiabetic levels by all three treatments. NOX is a major source of superoxide in the vascular endothelium, and NOX-mediated overproduction of ROS is involved in the initiation and progression of diabetic vascular complications by decreasing the bioavailability of nitric oxide (32,33). Inhibition of NOS-2 prevented diabetic vascular dysfunction in rats (34–36). Finally, both NOS-2 and NOX contribute to the accumulation of ROS, which causes senescence and impairs self-renewal of progenitor cells (37–40). These findings support our global hypothesis that marrow neuropathy manifests as microvascular complications by compromising the release and function of reparative progenitors. Accordingly, these findings support our overall hypothesis that the selected therapies improve the phenotype of bone marrow–derived progenitor cells, which attenuates diabetic microvascular complications.

Late-stage peripheral diabetic neuropathy is characterized by a loss of innervation (41,42); however, the early stages of injury in the T1D bone marrow may be associated with preemptive or compensatory neurogenesis. We observed that 8 weeks of STZ-induced diabetes was associated with an increased proportion of strong-positive immunoreactivity for all neural pathways investigated. This putative neurogenesis could be mediated by the local bone marrow microenvironment via an increase of neurotrophic factors. Trophic substances are supplied by the target tissue, and the relative abundance of trophic factors may regulate the density of innervation of the target (43). In fact, increased neuropeptide concentrations are observed in the early stages of diabetic inflammation (44,45).

We previously studied a T2D model that was associated with decreased TH and neurofilament 200 immunoreactivity in the marrow of the humerus (14). Here, in a T1D model, we observed an increase of strong-positive immunoreactivity for TH in the femur (Fig. 1*B*). The disparity

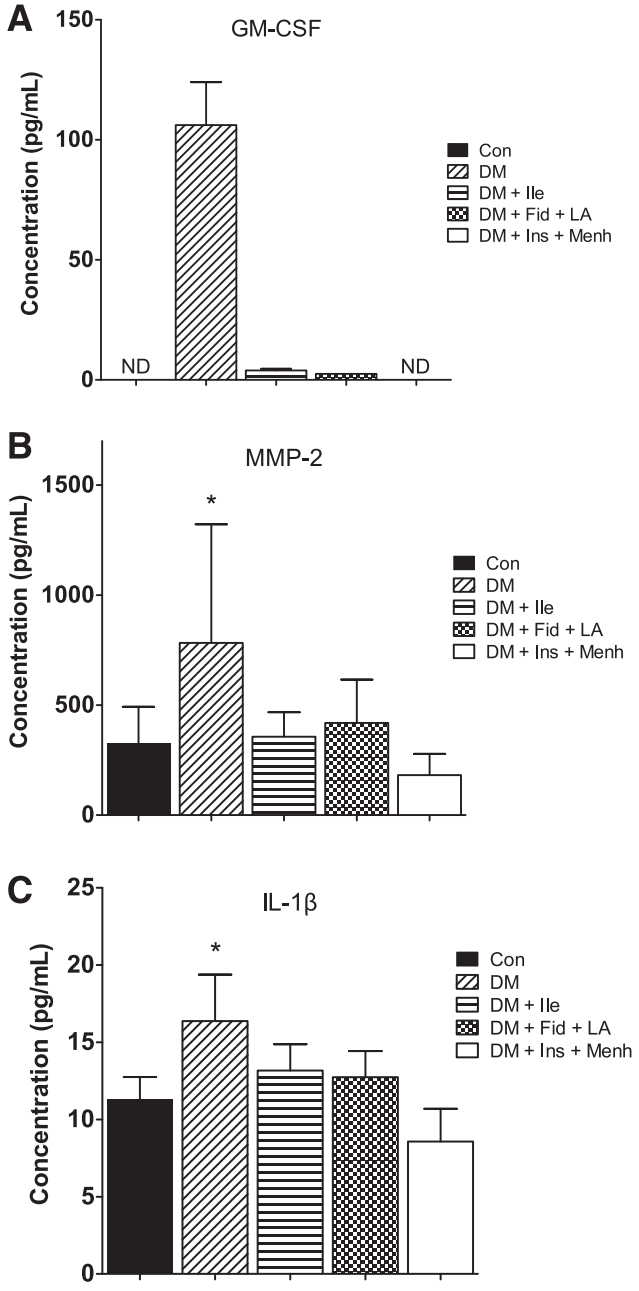

Figure 5—GM-CSF (*A*), MMP-2 (*B*), and IL-1β (*C*) in femoral marrow. Data represent mean ± SD. Statistics for GM-CSF (*A*) could not be applied because of low detection in the nondiabetic control (Con) and treatment groups. *Significant difference from all other groups ($P < 0.05$). ND, not detected.

between the two studies is likely due to differences in the etiology of STZ-induced diabetes and T2D. For example, insulin is effectively absent in STZ-induced/T1D, whereas the concentrations of insulin present in T2D may be sufficient to attenuate neuropathy (46,47). In fact, the magnitude of sympathetic neuroaxonal dystrophy is more severe in the STZ-induced diabetes than the T2D model (46), as predicted. Thus, it is possible that the severe neuropathic phenotype of the T1D model initiates a greater compensatory response, particularly in the early stages, which manifests as the observed increase in strong-positive immunoreactivity.

Another potential explanation for increased neurotransmitter expression early in STZ-induced diabetes is damage to neurons themselves. Injury (e.g., ischemic, mechanical, or epileptic) is well known to induce neurogenesis in various brain regions. Animal models of epilepsy exhibit neurogenesis in the dentate gyrus (22). In animal models of stroke, transient ischemia induces proliferation of progenitor cells that possess neuronal markers that were able to send axonal projections from the anterior cortex to the thalamus (21). We propose that a similar phenomenon consisting of early injury and compensatory neurogenesis occurs in the T1D bone marrow, which ultimately becomes inadequate and results in sustained injury, leading to denervation, characteristic of advanced diabetic neuropathy (41,42).

Tan et al. (48) provided an additional explanation for the STZ-induced diabetes–associated increase in strong-positive neurotransmitter immunoreactivity. They described a STZ-induced diabetes–associated increase in length and head diameter of dendritic spines and increased density of mushroom-shaped spines of second-order nociceptive neurons in the dorsal horn. These alterations presumably would increase the volume of each affected neuropeptide-containing dendrite, resulting in increased neurotransmitter content and increased immunoreactivity. In addition, these morphologic changes in dendritic spines were mechanistically linked to neuropathic pain (48).

Our results for SST are analogous to those of TH. SST functions as a chemoattractant for primitive hematopoietic progenitor cells (49) and controls differentiation and migration of thymocytes (50). Whereas noradrenergic activation facilitates release of progenitor cells to the circulation, SST release may function to sequester progenitor cells in the bone marrow. This is consistent with our finding that the bone marrow of rats with STZ-induced diabetes and T2D sequesters progenitor cell populations, as opposed to facilitating their cyclic, regulated release into the circulation (14).

SST decreased the viability of and chemokine production from both activated and unstimulated human macrophages (19). In addition, SST inhibits chemokine-induced T-cell infiltration through collagen, presumably by inhibiting secretion of MMPs (51). It is possible that the increased strong-positive SST immunoreactivity with STZ-induced diabetes (Fig. 2) occurs to suppress the proinflammatory milieu in the STZ-induced diabetic bone marrow (Fig. 5).

Similar to our immunoreactivity data for TH and SST, strong-positive NPY immunoreactivity was increased with STZ-induced diabetes and was maintained at control values in the treatment conditions. Fehér et al. (44) described an early increase in NPY-immunoreactive nerve fibers in the alimentary tract of STZ-induced diabetic rats. Similar to our interpretation, they suggested a compensatory

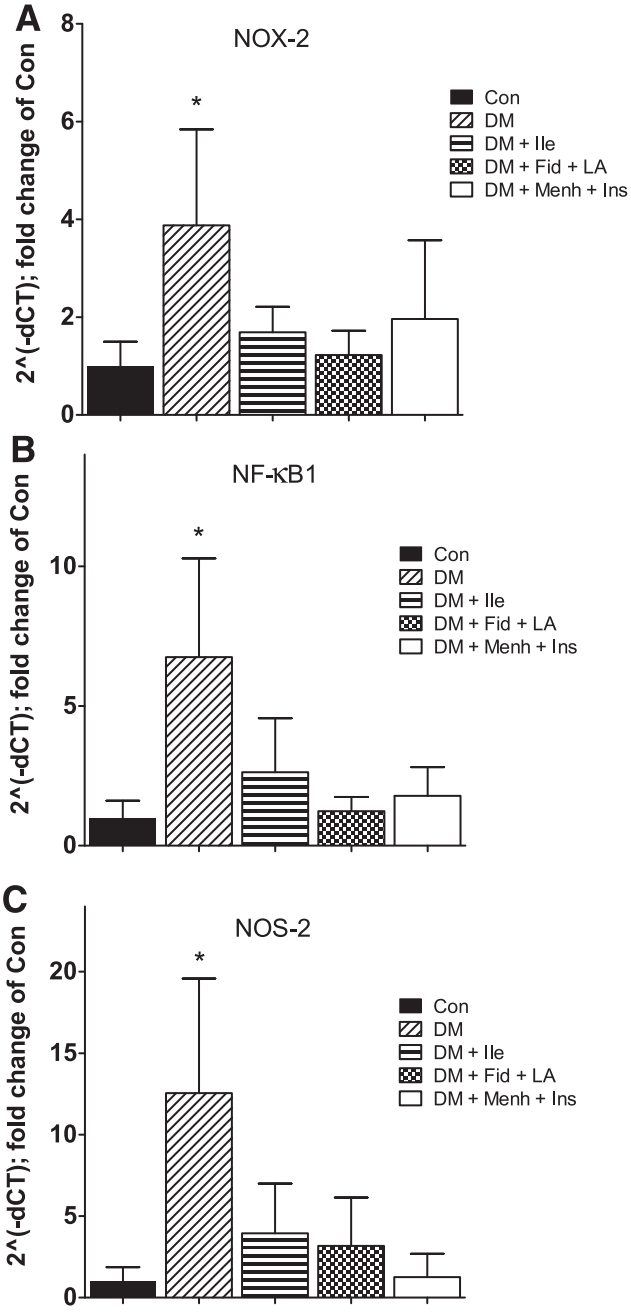

Figure 6—NOX-2 (*A*), NF-κB1 (*B*), and NOS-2 (*C*) gene expression from Thy1$^+$ cells isolated from femurs. Data represent mean ± SD. *Significant difference from all other groups ($P < 0.05$).

response to offset the depletion of neuropeptides associated with STZ-induced diabetes. Circulating NPY is elevated with chronic stress and sympathetic nervous system activation (52). However, NPY has curiously been shown to differentially influence the propagation of inflammation. For example, exogenous NPY decreases inflammation in sepsis models (53) and decreases activated macrophages (54) yet activates antigen-presenting cells (55). In addition, elevated NPY in the bone marrow may have beneficial effects in increasing progenitor cell populations and maintaining their undifferentiated status; NPY receptor type-1 activation was associated with increased mesenchymal progenitor cell populations (20).

In contrast to our findings, Garrett et al. (56) revealed an STZ-induced diabetes–associated decrease in NPY-like immunoreactivity in the sciatic nerve in a rat model of diabetic neuropathy (8 weeks), suggesting that neurogenesis may not occur in all peripheral nerves. However, similar to the current study, the STZ-induced diabetes–associated decrease described by Garrett et al. was attenuated by treatment with LA. On the other hand, Ahmad et al. (57) analyzed the femoral and tibial marrow and determined that 8 months of T2D significantly decreased NPY, as expected with longer durations of diabetes. They attributed loss of NPY to both neuronal and nonneuronal (i.e., megakaryocytes) sources. While the literature is divided between studies that reveal increased and decreased NPY with diabetes, the duration of diabetes, not the type, seems to be most accountable for the direction of change.

Another unexpected finding was that bone marrow adiposity was significantly decreased in the DM compared with the Con group but was increased with treatment in the Ile and Ins + Menh groups. Bone marrow adipose is proposed to have mixed white and brown fat characteristics (58,59). It has been hypothesized that the brown adipose-like phenotype provides energy for hematopoietic and mesenchymal compartments (60). Acting as autocrine/paracrine/endocrine support, lipid-filled adipocytes in the bone marrow repress growth and differentiation of hematopoietic stem cells (61,62) and have been considered negative regulators of the hematopoietic niche (60,63). This suppressive activity has been primarily attributed to the reduced production of GM-CSF and granulocyte colony-stimulating factor and increased secretion of neuropilin and lipocalin-2 (61,64). This is also consistent with our finding that DM was associated with decreased marrow adiposity and increased GM-CSF.

This study demonstrates that the bone marrow may be a therapeutic target. We showed that early in STZ-induced diabetes, the bone marrow is characterized by an increased proportion of strong-positive immunoreactivity for TH, SST, and NPY; decreased bone marrow adiposity; a highly proinflammatory bone marrow microenvironment; and increased proinflammatory gene expression in bone marrow–derived progenitor cells. Vasopeptidase inhibition or combination treatments to inhibit aldose reductase and decrease oxidative stress or supplementation with ω-3 PUFAs and insulin prevented functional neuronal defects and damage to the bone marrow caused by STZ-induced diabetes. Follow-up studies of these therapeutic strategies should include assessment of progenitor cell function and examination in T2D models. Furthermore, in a clinical setting, these treatment conditions could be combined (e.g., Ins + Fid + Ile + LA), and determining whether an additive effect exists will be

important because these agents address independent pathways known to be dysfunctional in diabetes.

Acknowledgments. The authors thank Amy S. Porter, Kathleen A. Joseph, and Katlyn M. Welch, of the Investigative HistoPathology Laboratory at Michigan State University, for their expertise with bone histology. The authors also thank Dr. Ann Fu of the Molecular Pathology Core at the University of Florida for her assistance with the Aperio system.

Funding. This material is based on work supported in part by the Department of Veterans Affairs, Veterans Health Administration, Office of Research and Development, Biomedical Laboratory Research and Development (grant BX001680).

Duality of Interest. No potential conflicts of interest relevant to this article were reported.

Author Contributions. J.M.D. performed bone marrow and cell experiments and PCR, analyzed data, and wrote the manuscript. M.A.Y. cared for the animals, performed nerve conduction experiments, and processed bones. M.B.G. designed experiments and wrote the manuscript. M.B.G. is the guarantor of this work and, as such, had full access to all the data in the study and takes responsibility for the integrity of the data and the accuracy of the data analysis.

References

1. Centers for Disease Control and Prevention. *National Diabetes Statistics Report: Estimates of Diabetes and its Burden in the United States, 2014.* Atlanta, GA, U.S. Department of Health and Human Services, 2014

2. Ziegler-Graham K, MacKenzie EJ, Ephraim PL, Travison TG, Brookmeyer R. Estimating the prevalence of limb loss in the United States: 2005 to 2050. Arch Phys Med Rehabil 2008;89:422–429

3. Judzewitsch RG, Jaspan JB, Polonsky KS, et al. Aldose reductase inhibition improves nerve conduction velocity in diabetic patients. N Engl J Med 1983;308: 119–125

4. Davidson EP, Kleinschmidt TL, Oltman CL, Lund DD, Yorek MA. Treatment of streptozotocin-induced diabetic rats with AVE7688, a vasopeptidase inhibitor: effect on vascular and neural disease. Diabetes 2007;56:355–362

5. Coppey LJ, Gellett JS, Davidson EP, Dunlap JA, Yorek MA. Effect of treating streptozotocin-induced diabetic rats with sorbinil, myo-inositol or aminoguanidine on endoneurial blood flow, motor nerve conduction velocity and vascular function of epineurial arterioles of the sciatic nerve. Int J Exp Diabetes Res 2002;3:21–36

6. Gonzalez AM, Sochor M, McLean P. The effect of an aldose reductase inhibitor (Sorbinil) on the level of metabolites in lenses of diabetic rats. Diabetes 1983;32:482–485

7. Busse E, Zimmer G, Schopohl B, Kornhuber B. Influence of alpha-lipoic acid on intracellular glutathione in vitro and in vivo. Arzneimittelforschung 1992;42: 829–831

8. Low PA, Nickander KK, Tritschler HJ. The roles of oxidative stress and antioxidant treatment in experimental diabetic neuropathy. Diabetes 1997;46 (Suppl. 2):S38–S42

9. Nagamatsu M, Nickander KK, Schmelzer JD, et al. Lipoic acid improves nerve blood flow, reduces oxidative stress, and improves distal nerve conduction in experimental diabetic neuropathy. Diabetes Care 1995;18:1160–1167

10. Sola S, Mir MQ, Cheema FA, et al. Irbesartan and lipoic acid improve endothelial function and reduce markers of inflammation in the metabolic syndrome: results of the Irbesartan and Lipoic Acid in Endothelial Dysfunction (ISLAND) study. Circulation 2005;111:343–348

11. De Caterina R, Madonna R, Bertolotto A, Schmidt EB. n-3 fatty acids in the treatment of diabetic patients: biological rationale and clinical data. Diabetes Care 2007;30:1012–1026

12. Katayama Y, Battista M, Kao WM, et al. Signals from the sympathetic nervous system regulate hematopoietic stem cell egress from bone marrow. Cell 2006;124:407–421

13. Hazra S, Jarajapu YP, Stepps V, et al. Long-term type 1 diabetes influences haematopoietic stem cells by reducing vascular repair potential and increasing inflammatory monocyte generation in a murine model. Diabetologia 2013;56: 644–653

14. Busik JV, Tikhonenko M, Bhatwadekar A, et al. Diabetic retinopathy is associated with bone marrow neuropathy and a depressed peripheral clock. J Exp Med 2009;206:2897–2906

15. Hu P, Thinschmidt JS, Yan Y, et al. CNS inflammation and bone marrow neuropathy in type 1 diabetes. Am J Pathol 2013;183:1608–1620

16. Coppey LJ, Holmes A, Davidson EP, Yorek MA. Partial replacement with menhaden oil improves peripheral neuropathy in high-fat-fed low-dose streptozotocin type 2 diabetic rat. J Nutr Metab2012;2012:950517

17. Nagatsu T, Levitt M, Udenfriend S. Tyrosine hydroxylase. The initial step in norepinephrine biosynthesis. J Biol Chem 1964;239:2910–2917

18. Chalazonitis A, Zigmond RE. Effects of synaptic and antidromic stimulation on tyrosine hydroxylase activity in the rat superior cervical ganglion. J Physiol 1980;300:525–538

19. Armani C, Catalani E, Balbarini A, Bagnoli P, Cervia D. Expression, pharmacology, and functional role of somatostatin receptor subtypes 1 and 2 in human macrophages. J Leukoc Biol 2007;81:845–855

20. Lundberg P, Allison SJ, Lee NJ, et al. Greater bone formation of Y2 knockout mice is associated with increased osteoprogenitor numbers and altered Y1 receptor expression. J Biol Chem 2007;282:19082–19091

21. Magavi SS, Leavitt BR, Macklis JD. Induction of neurogenesis in the neocortex of adult mice. Nature 2000;405:951–955

22. Parent JM, Yu TW, Leibowitz RT, Geschwind DH, Sloviter RS, Lowenstein DH. Dentate granule cell neurogenesis is increased by seizures and contributes to aberrant network reorganization in the adult rat hippocampus. J Neurosci 1997; 17:3727–3738

23. Seo JY, Kim H, Kim KH. Transcriptional regulation by thiol compounds in Helicobacter pylori-induced interleukin-8 production in human gastric epithelial cells. Ann N Y Acad Sci 2002;973:541–545

24. Ramana KV, Willis MS, White MD, et al. Endotoxin-induced cardiomyopathy and systemic inflammation in mice is prevented by aldose reductase inhibition. Circulation 2006;114:1838–1846

25. Morcos M, Borcea V, Isermann B, et al. Effect of alpha-lipoic acid on the progression of endothelial cell damage and albuminuria in patients with diabetes mellitus: an exploratory study. Diabetes Res Clin Pract 2001;52:175–183

26. Matsumoto M, Sata M, Fukuda D, et al. Orally administered eicosapentaenoic acid reduces and stabilizes atherosclerotic lesions in ApoE-deficient mice. Atherosclerosis 2008;197:524–533

27. Sorgi CA, Rose S, Court N, et al. GM-CSF priming drives bone marrow-derived macrophages to a pro-inflammatory pattern and downmodulates PGE2 in response to TLR2 ligands. PLoS One 2012;7:e40523

28. Lacey DC, Achuthan A, Fleetwood AJ, et al. Defining GM-CSF- and macrophage-CSF-dependent macrophage responses by in vitro models. J Immunol 2012;188:5752–5765

29. Fleetwood AJ, Lawrence T, Hamilton JA, Cook AD. Granulocyte-macrophage colony-stimulating factor (CSF) and macrophage CSF-dependent macrophage phenotypes display differences in cytokine profiles and transcription factor activities: implications for CSF blockade in inflammation. J Immunol 2007;178: 5245–5252

30. Agro A, Jordana M, Chan KH, et al. Synoviocyte derived granulocyte macrophage colony stimulating factor mediates the survival of human lymphocytes. J Rheumatol 1992;19:1065–1069

31. Alvaro-Gracia JM, Zvaifler NJ, Brown CB, Kaushansky K, Firestein GS. Cytokines in chronic inflammatory arthritis. VI. Analysis of the synovial cells involved in granulocyte-macrophage colony-stimulating factor production and gene expression in rheumatoid arthritis and its regulation by IL-1 and tumor necrosis factor-alpha. J Immunol 1991;146:3365–3371

32. Guzik TJ, Mussa S, Gastaldi D, et al. Mechanisms of increased vascular superoxide production in human diabetes mellitus: role of NAD(P)H oxidase and endothelial nitric oxide synthase. Circulation 2002;105:1656–1662

33. Hink U, Li H, Mollnau H, et al. Mechanisms underlying endothelial dysfunction in diabetes mellitus. Circ Res 2001;88:E14–E22
34. Nagareddy PR, Xia Z, McNeill JH, MacLeod KM. Increased expression of iNOS is associated with endothelial dysfunction and impaired pressor responsiveness in streptozotocin-induced diabetes. Am J Physiol Heart Circ Physiol 2005;289:H2144–H2152
35. Gunnett CA, Lund DD, Chu Y, Brooks RM 2nd, Faraci FM, Heistad DD. NO-dependent vasorelaxation is impaired after gene transfer of inducible NO-synthase. Arterioscler Thromb Vasc Biol 2001;21:1281–1287
36. Gunnett CA, Heistad DD, Faraci FM. Gene-targeted mice reveal a critical role for inducible nitric oxide synthase in vascular dysfunction during diabetes. Stroke 2003;34:2970–2974
37. Ito K, Hirao A, Arai F, et al. Reactive oxygen species act through p38 MAPK to limit the lifespan of hematopoietic stem cells. Nat Med 2006;12:446–451
38. Urao N, Inomata H, Razvi M, et al. Role of nox2-based NADPH oxidase in bone marrow and progenitor cell function involved in neovascularization induced by hindlimb ischemia. Circ Res 2008;103:212–220
39. Jang YY, Sharkis SJ. A low level of reactive oxygen species selects for primitive hematopoietic stem cells that may reside in the low-oxygenic niche. Blood 2007;110:3056–3063
40. Piccoli C, D'Aprile A, Ripoli M, et al. Bone-marrow derived hematopoietic stem/progenitor cells express multiple isoforms of NADPH oxidase and produce constitutively reactive oxygen species. Biochem Biophys Res Commun 2007;353:965–972
41. Tack CJ, van Gurp PJ, Holmes C, Goldstein DS. Local sympathetic denervation in painful diabetic neuropathy. Diabetes 2002;51:3545–3553
42. Britland ST, Young RJ, Sharma AK, Clarke BF. Association of painful and painless diabetic polyneuropathy with different patterns of nerve fiber degeneration and regeneration. Diabetes 1990;39:898–908
43. Korsching S, Thoenen H. Developmental changes of nerve growth factor levels in sympathetic ganglia and their target organs. Dev Biol 1988;126:40–46
44. Fehér E, Batbayar B, Vér A, Zelles T. Changes of the different neuropeptide-containing nerve fibers and immunocells in the diabetic rat's alimentary tract. Ann N Y Acad Sci 2006;1084:280–295
45. Donnerer J, Schuligoi R, Stein C. Increased content and transport of substance P and calcitonin gene-related peptide in sensory nerves innervating inflamed tissue: evidence for a regulatory function of nerve growth factor in vivo. Neuroscience 1992;49:693–698
46. Schmidt RE, Dorsey DA, Beaudet LN, Parvin CA, Zhang W, Sima AA. Experimental rat models of types 1 and 2 diabetes differ in sympathetic neuroaxonal dystrophy. J Neuropathol Exp Neurol 2004;63:450–460
47. Schmidt RE, Dorsey DA, Beaudet LN, Peterson RG. Analysis of the Zucker Diabetic Fatty (ZDF) type 2 diabetic rat model suggests a neurotrophic role for insulin/IGF-I in diabetic autonomic neuropathy. Am J Pathol 2003;163:21–28
48. Tan AM, Samad OA, Fischer TZ, Zhao P, Persson AK, Waxman SG. Maladaptive dendritic spine remodeling contributes to diabetic neuropathic pain. J Neurosci 2012;32:6795–6807
49. Oomen SP, van Hennik PB, Antonissen C, et al. Somatostatin is a selective chemoattractant for primitive (CD34(+)) hematopoietic progenitor cells. Exp Hematol 2002;30:116–125
50. Solomou K, Ritter MA, Palmer DB. Somatostatin is expressed in the murine thymus and enhances thymocyte development. Eur J Immunol 2002;32:1550–1559
51. Talme T, Ivanoff J, Sundqvist KG. Somatostatin is a specific inhibitor of SDF-1alpha-induced T cell infiltration. Clin Exp Immunol 2004;135:434–439
52. Lambert GW, Straznicky NE, Lambert EA, Dixon JB, Schlaich MP. Sympathetic nervous activation in obesity and the metabolic syndrome—causes, consequences and therapeutic implications. Pharmacol Ther 2010;126:159–172
53. Bedoui S, Miyake S, Lin Y, et al. Neuropeptide Y (NPY) suppresses experimental autoimmune encephalomyelitis: NPY1 receptor-specific inhibition of autoreactive Th1 responses in vivo. J Immunol 2003;171:3451–3458
54. Singer K, Morris DL, Oatmen KE, et al. Neuropeptide Y is produced by adipose tissue macrophages and regulates obesity-induced inflammation. PLoS One 2013;8:e57929
55. Wheway J, Herzog H, Mackay F. The Y1 receptor for NPY: a key modulator of the adaptive immune system. Peptides 2007;28:453–458
56. Garrett NE, Malcangio M, Dewhurst M, Tomlinson DR. alpha-Lipoic acid corrects neuropeptide deficits in diabetic rats via induction of trophic support. Neurosci Lett 1997;222:191–194
57. Ahmad T, Ugarph-Morawski A, Li J, et al. Bone and joint neuropathy in rats with type-2 diabetes. Regul Pept 2004;119:61–67
58. Krings A, Rahman S, Huang S, Lu Y, Czernik PJ, Lecka-Czernik B. Bone marrow fat has brown adipose tissue characteristics, which are attenuated with aging and diabetes. Bone 2012;50:546–552
59. Gimble JM, Nuttall ME. Bone and fat: old questions, new insights. Endocrine 2004;23:183–188
60. Lecka-Czernik B. Marrow fat metabolism is linked to the systemic energy metabolism. Bone 2012;50:534–539
61. Naveiras O, Nardi V, Wenzel PL, Hauschka PV, Fahey F, Daley GQ. Bone-marrow adipocytes as negative regulators of the haematopoietic microenvironment. Nature 2009;460:259–263
62. Gimble JM, Nuttall ME. The relationship between adipose tissue and bone metabolism. Clin Biochem 2012;45:874–879
63. Omatsu Y, Sugiyama T, Kohara H, et al. The essential functions of adipo-osteogenic progenitors as the hematopoietic stem and progenitor cell niche. Immunity 2010;33:387–399
64. Belaid-Choucair Z, Lepelletier Y, Poncin G, et al. Human bone marrow adipocytes block granulopoiesis through neuropilin-1-induced granulocyte colony-stimulating factor inhibition. Stem Cells 2008;26:1556–1564